J. Fluid Mech. (1984), *vol.* 148, *pp.* 271–284
Printed in Great Britain

Drag on a sphere moving horizontally through a stratified liquid

By KARL E. B. LOFQUIST AND L. PATRICK PURTELL
National Bureau of Standards, Gaithersburg, MD 20899

(Received 11 November 1981 and in revised form 7 June 1984)

The drag on a sphere moving horizontally through stably stratified salt water is measured in laboratory experiments. The increment ΔC_D in drag coefficient due to the stratification is obtained as a function of a stratification parameter κ and, in principle, the usual Reynolds number R. In these experiments, where R ranges from 150 to 5000, ΔC_D is insensitive to R. But, as a function of κ, ΔC_D has both positive and negative values attributable respectively to lee-wave drag and to suppression of turbulence in the wake. An observed delay in flow separation also apparently results from the lee-wave drag.

1. Introduction

This paper describes measurements of drag on a sphere moving with constant horizontal velocity through a stably stratified liquid. If, as in the present case, the boundaries of the liquid are so distant as to have negligible effect on the drag D, and if the stratification can be specified by a single quantity and does not significantly affect the kinematic viscosity ν, the drag coefficient becomes a function only of the usual Reynolds number and one other dimensionless quantity. In particular, with the density ρ determined as a function of the vertical coordinate z by a constant Brunt–Väisälä angular frequency

$$N = \left(\frac{-g}{\rho}\frac{\mathrm{d}\rho}{\mathrm{d}z}\right)^{\frac{1}{2}} \quad \text{a constant} \tag{1}$$

with ρ_0 the density of the undisturbed liquid at the level of the sphere's centre, and with V the velocity of the sphere, the coefficient

$$C_D(R,\kappa) = \frac{2D}{\pi a^2 \rho_0 V^2} \tag{2}$$

is a function of

$$R = \frac{2aV}{\nu} \quad \text{and} \quad \kappa = \frac{Na}{V}. \tag{3), (4}$$

An 'internal' Froude number $F = 1/2\kappa$ is sometimes used. The function $C_D(R,\kappa)$ is a generalization of the coefficient $C_D(R,0)$ for unstratified drag. The present measurements provide $C_D(R,\kappa)$ over the approximate ranges $1.5\times10^2 < R < 5\times10^3$, $0.1 < \kappa < 10$.

We are unaware of any previous similar measurements of stratified drag, over any range of κ. Therefore past work will be described as it applies in particular, without a general summary.

2. The experimental programme

As shown in figure 1, a sphere, suspended by fine thread from a movable carriage, was pulled through stably stratified salt water. In steady motion, the thread inclined from the vertical by an angle θ_0, in air, making vertical and horizontal tensile forces at the water's surface balance the submerged weight W of the sphere and the sum of the drags of the sphere and of the thread, D and d respectively. That is,

$$D + d = W \tan \theta_0. \tag{5}$$

With stratification, the submerged weight of the sphere depended upon both its own density and its elevation. Before an experiment, W was measured with the sphere at rest at the fixed elevation of mid-depth. During subsequent motion, the angle θ_0 was observed while the thread was reeled out enough to keep the elevation and submerged weight of the sphere nearly unchanged.

2.1. *Apparatus*

The tank was 15.7 m (40 ft) long and 0.96 (3 ft) wide, and was filled to a depth of 50 cm. The carriage rode on tracks atop the tank walls, towed at selected speeds by a variable-speed electric motor. The sphere was 6.36 cm (≈ 2.5 in.) in diameter and made of Plexiglas. Its density was adjusted by loading lead shot or mercury into a water-filled central cavity with a removable cap. Smaller sealed air-filled cavities reduced the specific gravity to slightly less than 1.0 with the central cavity unloaded. The sphere was suspended at mid-depth by nylon thread, 0.127 mm (0.005 in.) in diameter, attached to the carriage at points 118 cm above. There were, in fact, two threads, 3.0 cm apart where they were attached to the sphere and spreading laterally as they ascended to 78 cm apart at the carriage, thus preventing lateral sway. The rearward rotation θ_0 of the threads about their point of suspension was read on a scale midway between them and just above the free surface. This was marked with segments of radii through the point of suspension for selected values of $10^2 \tan \theta_0$, and against this scale the nearer thread was observed while keeping both threads aligned to avoid parallax. The threads remained nearly straight, even in the water, which permitted a reel and scale to be devised whereby, for any observed θ_0, the threads could be reeled in or out to keep the elevation of the sphere nearly constant. The submerged weight was measured with the sphere at rest by deflections of calibrated wires and springs from which the threads were temporarily suspended.

2.2. *Stratification*

The stratified salt water was laid down in 16 layers, with an overnight diffusion allowed to provide an initially nearly linear density profile. Continuous diffusion and frequent overturning and mixing in the liquid adjacent to the free surface and the bottom formed layers of nearly constant densities, usually with visible interfaces, above and below the stratified liquid. From day to day, the outer layers swelled as the inner region of nearly constant density gradient shrank. Depending upon $\Delta\rho/\rho_0$ and circumstance, fillings of the tank were made to serve from 4 to 17 days.

2.3. *Running the experiments*

Before an experiment, the sphere was weighted with lead shot, or with mercury, and weighed in position as described above. The carriage was then moved to one end of the tank, which consisted of ten sections. After currents in the water had apparently died out, at a selected setting of the motor, the carriage was quickly set into motion,

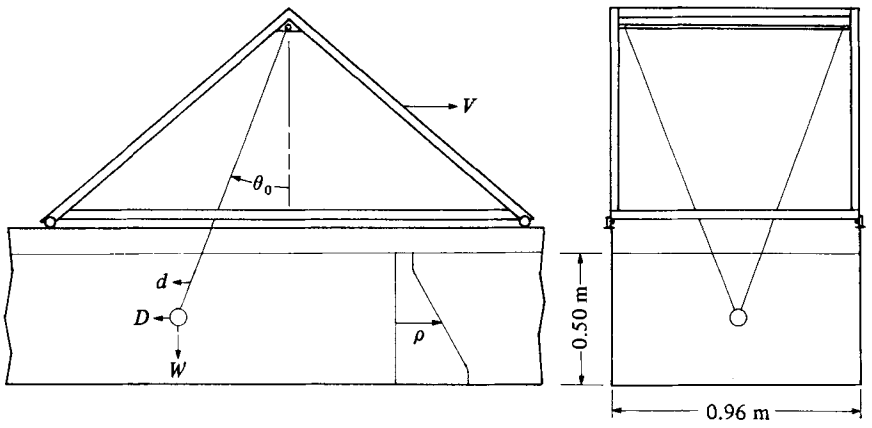

FIGURE 1. Diagrams of longitudinal and cross-sections of the tank, carriage and sphere. A density profile and the balance of forces are indicated.

towed at a constant speed to the other end, and quickly stopped. Speed was determined by a stopwatch. The sphere accelerated and decelerated quickly and smoothly, within the first and last end sections, and moved through the eight centre sections nearly steadily and usually without noticeable longitudinal oscillations. An observer walking alongside keeping an eye aligned with the two threads was able to make eight observations of θ_0, each a mental average over the length of one section. Since θ_0 held fairly constant, it was not difficult, with a little practice, to adjust the reel and hold the sphere at nearly constant elevation. After about half an hour, a pass was repeated in the opposite direction, to average out effects of possible undetected currents, and an average θ_0 was obtained from the 16 observations. The number of passes per experiment was regularly two, sometimes several, and rarely only one.

2.4. *Range of the experiments*

In figure 2 each of the more than 300 experiments is plotted by its values of the independent variables R and κR. The product κR is useful since it is independent of V and serves as a measure of the stratification. Thus for a given filling of the tank all experiments have the same κR. Denoting the difference in density between bottom and top layers by $\Delta\rho$, and taking ν as 10^{-2} cm^2 s^{-1}, values of $\Delta\rho/\rho_0$ have been entered along the right margin of the plot. Some experiments were carried out with fresh water. With $\kappa R = 0$ these could not be included on the logarithmic plot, but are shown plotted according to their values of R along a separate line below. Except for concentrations at selected values of $\Delta\rho/\rho_0$, the experiments are fairly evenly distributed within a region bounded by constant values of R and κR.

These boundaries were set by circumstance. Higher values of κR were not attained because of their demand for salt (it took 250 kg to fill the tank for $\Delta\rho/\rho_0 = 0.06$). Reliable observations of drag required that $\tan\theta_0 \sim D/W$ remain, roughly, between 0.05 and 0.20. With R increased beyond about 5×10^3, D became so large that W could not be made large enough, even with the sphere filled to capacity with mercury. And, with R reduced below about 170, D and W both became so small that the threads began to sag while W became increasingly sensitive to the elevation of the sphere in the stratified water. Also, at low values of R, longitudinal oscillations of the sphere became troublesome. However, stratification reduced these oscillations and permitted observations at lower values of R than could be attained in fresh water.

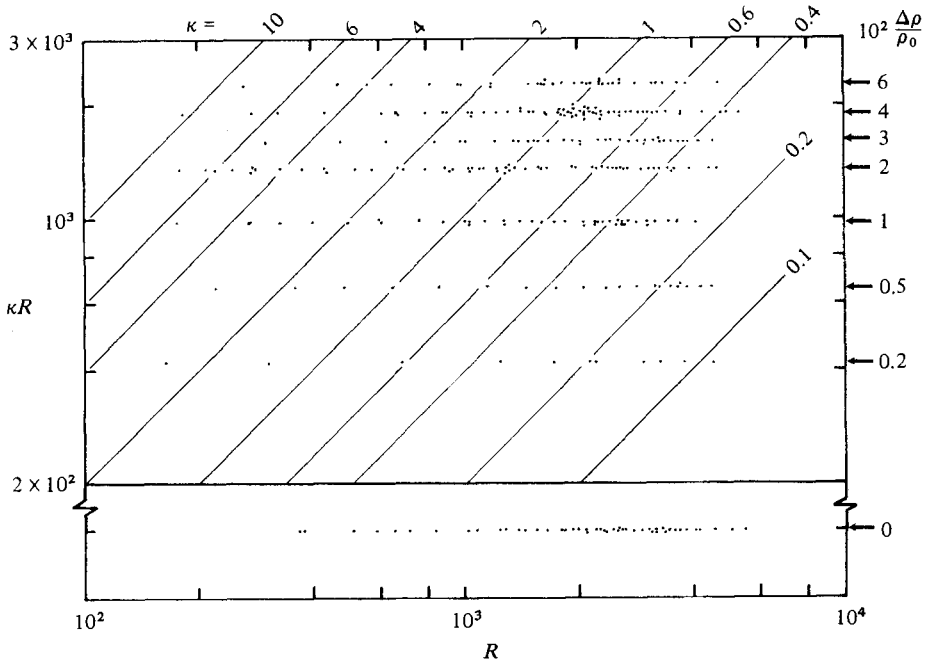

FIGURE 2. Distribution of the experiments. Each experiment is identified by values of the independent variables R and κ, the Reynolds number and stratification parameter (4). Values of κR and approximately corresponding values of $\Delta\rho/\rho_0$ are also shown.

3. Results

3.1. C'_D as a function of R and κR

Replacing D in (2) by $D+d$ defines a new coefficient $C'_D(R,\kappa)$, which includes the drag of the thread. In figure 3, for all the experiments, C'_D is plotted as a function of R with κR as a parameter, a curve drawn for each discrete value of κR that occurs. The curve $\kappa R = 0$, the non-stratified case, is drawn with heavier line. It appears that in most cases, over the greater range of R, stratification increased the drag, by as much as twice, but also, in the region of higher R, stratification reduced the drag, by as much as $\frac{1}{7}$. These effects are discussed in §4. In parts of figure 3 sinuosities in the curves may appear too refined for the data. All these curves have been constructed from $C'_D(R,0)$ in figure 3 and $\Delta C_D(R,\kappa)$ in figure 4 by the use of (6).

3.2. *Cancelling the effect of the threads*

To obtain $C_D(R,\kappa)$ from $C'_D(R,\kappa)$ it is necessary to subtract the effect of the threads. $C'_D(R,0)$ in figure 3 ranges, as R decreases, from about 25 % to 100 % higher than the unstratified $C_D(R)$ given in Schlichting (1968). Since $\tan\theta_0$ is always less than 0.24, and is typically around 0.1, the threads are sufficiently vertical to presume that fluid motions in their wakes are horizontal and that d is insensitive to stratification. Then d cancels out in taking the difference

$$C'_D(R,\kappa) - C'_D(R,0) = C_D(R,\kappa) - C_D(R,0) \equiv \Delta C_D(R,\kappa), \tag{6}$$

so that $C_D(R,\kappa)$ is the sum of the observed $\Delta C_D(R,\kappa)$ and a given $C_D(R,0)$. In the present study, $\Delta C_D(R,\kappa)$, which isolates the effects of stratification, is of primary interest.

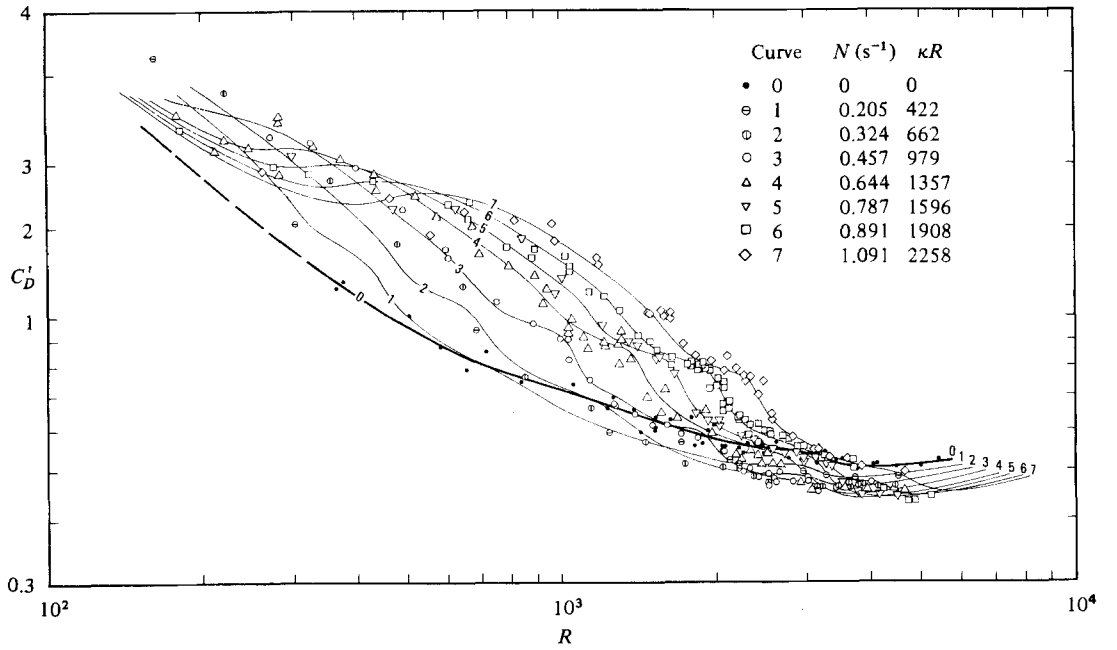

FIGURE 3. The drag coefficient C_D' as a function of Reynolds number R and stratification parameter κ (4). C_D' includes the resistance of the threads. Curves are drawn for selected values of κR. The curve for $\kappa R = 0$, the unstratified case, is drawn with a heavier line.

3.3. ΔC_D *as a function of* κ

In figure 4, ΔC_D has been plotted against κ. Here R enters as a parameter, but its effects are too small to be detected within the scatter. The function $\Delta C_D(\kappa)$ defines two regions, one positive and the other negative, for larger and smaller values of κ. Superposed on the larger positive hump are two or three smaller undulations. Although their amplitudes are within the range of scatter, their presence is confirmed by the numerous experiments purposely concentrated best to explore them. General features of the function $\Delta C_D(\kappa)$, its positive and negative regions, and its insensitivity to R, are discussed in §4.

3.4. *Observations of the wake and of flow separation*

An arclight outside the tank, at the elevation of the sphere or overhead, provided side- or topview shadowgraphs of the wake. In the first case, the shadow was projected onto a screen outside the tank on the far side inclined 45° from the vertical. In the second, the shadow was projected onto the submerged bottom of the tank. The topview shadowgraphs, being relatively obscure, were supplemented by photographs of streaklines of dye injected ahead of the sphere and swept into its wake. In all cases, the camera was mounted overhead. Patterns of the waves and wake are revealed by the envelope which separates at the sphere and encloses the partially mixed wake. Similar shadowgraphs have been made by Debler & Fitzgerald (1971). Representative shadowgraphs are shown in figure 5, all for $\Delta\rho/\rho_0 = 0.06$. The six sideviews include shadows of vertical threads, 10 cm apart, attached to the tank wall nearest the screen. Their angles and the elliptical shadows of the sphere reveal a distortion increasing with the angle between the ray producing the shadow and the perpendicular to the tank wall. These six shadowgraphs are arranged in two columns in order of increasing

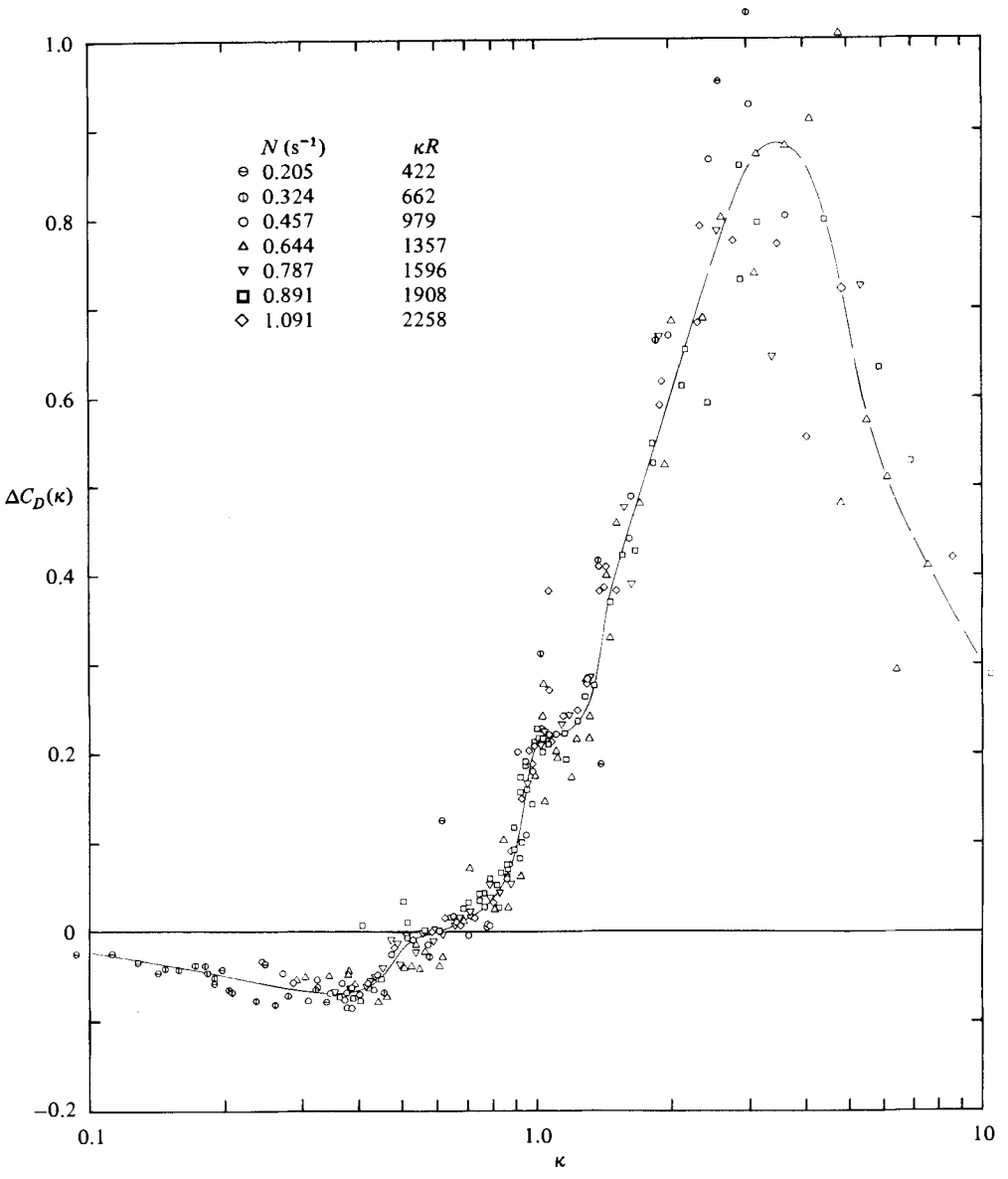

FIGURE 4. The change ΔC_D in the drag coefficient due to stratification, as a function of the stratification parameter κ (4). No effect of Reynolds number is apparent. Both increases and decreases in drag are observed.

R and decreasing κ. Paired with the last three sideview shadowgraphs, at approximately equal values of R and κ, are topviews (showing the sphere above its shadow).

Thirty-six sideview shadographs were distributed between $\Delta\rho/\rho_0 = 0.02$, 0.03 and 0.06. Their patterns of lee waves and wake advanced steadily with the sphere, with only minor unsteadiness associated with turbulence at higher values of R. Their character was found to be determined primarily by κ. As in the examples, as κ decreases from highest values, undulations on a thick envelope, nearly symmetrical above and below, lengthen and grow, to reach a maximum amplitude at some κ around 1.5. As κ continues to decrease, the undulations continue to lengthen but

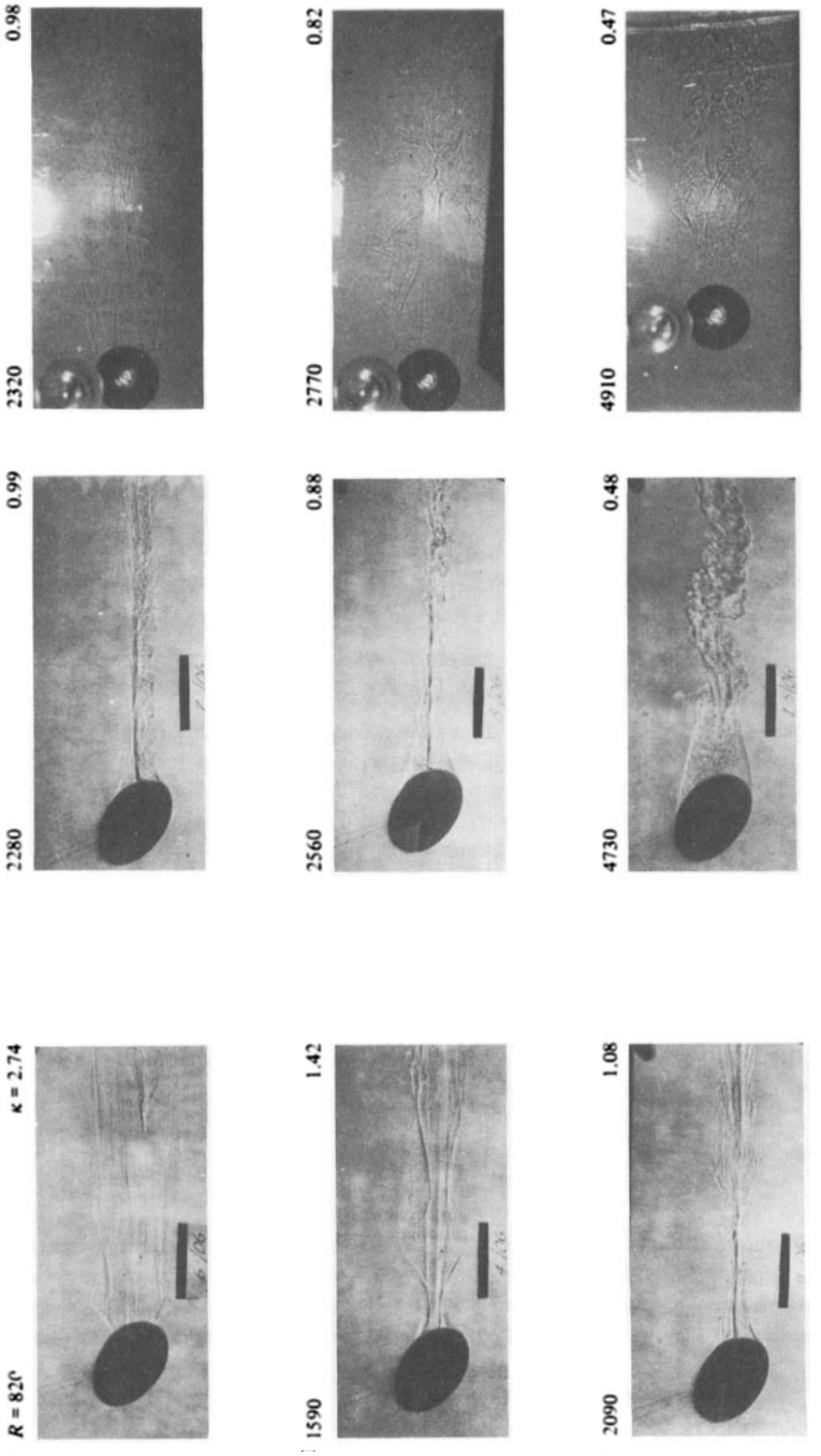

FIGURE 5. Shadowgraphs of the wake at selected values of R and κ. The two columns at the right are sideview and topview pairs, at approximately equal values of R and κ, to show how stratification inhibits the vertical spreading of the wake.

dwindle, as the wake flattens, effectively to disappear at some κ slightly below 1.0. As κ decreases still further, an increase in mixing, enhanced by increasing R with given κ, again thickens the wake, which regains an undulatory, essentially steady, character but not vertical symmetry. Thirteen topview shadowgraphs and nine dye streakline photographs were distributed between $\Delta\rho/\rho_0 = 0.03$ and 0.06. Here, for several diameters behind the sphere, the wakes remained wide compared with their compressed vertical sections, as may be seen in the three examples. Farther downstream (not shown), the wakes developed an unsteady but regular lateral sinuosity, like a two-dimensional vortex street behind a vertical cylinder, as described by Pao & Kao (1977).

Points where the flow separated from the sphere could be observed in most of the side- and topview photographs of the wake and identified by their angles ϕ behind the foremost point of the sphere. These photographs were supplemented by 19 sideview shadowgraph close-ups with light rays nearly perpendicular to the tank wall, and relatively undistorted. For each sideview, the average of the upper and lower ϕ is shown, by the open symbols, plotted against κ in figure 6. Symbols and values of $\Delta\rho/\rho_0$ are as in figures 3 and 4, with flags added to denote close-ups. The upper separation point was consistently delayed beyond the lower, the difference in ϕ ranging from 1° to 22°, with the average of around 11°. Figure 6 also contains the average ϕ for each of the topviews, plotted with solid symbols and with bars denoting the dye streakline observations. Both sets of data are discussed in §5, and remarks on the determination and accuracy of ϕ are included in §4.

4. Discussion of errors

A general assessment of the errors in measuring ΔC_D in these experiments can be had from the scatter in figure 4. Further specification is provided by analysis of δ, the displacement of an observed ΔC_D from the curve that has been drawn, in terms of its average $\bar{\delta}$ and standard deviation $\sigma(\delta)$, for various categories of experiments. Table 1 contains $\bar{\delta}$ and $\sigma(\delta)$ for several such categories, each subdivided for $\kappa < 1$ and $\kappa \geqslant 1$. The first column is for all the experiments in figure 4, and the other categories are introduced in §4.3. Other measures of error, not contained in the table, are discussed in §§4.1 and 4.2. The section ends with remarks on possible errors in the angle of separation.

4.1. *Curvature of the thread*

In the liquid, resistance to the thread causes it to curve slightly downward. With s the distance along the wetted thread from the free surface, and $s_1 - a$ its length to the surface of the sphere, the local inclination of the thread from the vertical is approximately

$$\tan\theta = \tan\theta_0 - \frac{d}{W}\frac{s}{s_1}, \tag{7}$$

with $\tan\theta_0$ as in (5). (Thus, were it practical, d/W could be determined by simultaneous observations of $\tan\theta$ at the free surface and at the sphere.) Since s_1 has been selected to make $s_1\cos\theta_0 = z_1$, the mid-depth, the curvature of the thread allows the centre of the sphere to sink a distance $|\Delta z|$ below mid-depth. Neglecting higher orders of d/W,

$$|\Delta z| = \frac{z_1}{2}\frac{d}{W}\sin\theta_0\cos\theta_0. \tag{8}$$

This displacement, with the stratification, reduces the submerged weight of the sphere by an amount

$$|\Delta W| = \tfrac{4}{3}\pi a^3 \rho_0 N^2 |\Delta z|, \tag{9}$$

thereby implying an equal overestimate of W and, by (5), a corresponding overestimate of D approximately equal to $|\Delta W| \tan\theta_0$. The overestimate of ΔC_D due to curving of the thread, denoted by $\delta_1 \Delta C_D$, is then approximately

$$\delta_1 \Delta C_D = \frac{4}{3}\frac{z_1}{a}\kappa^2 \frac{d}{D+d}\sin^2\theta_0 \tan\theta_0. \tag{10}$$

With an additional curve of $C_D(R,0)$ from Schlichting (1968), $d/(D+d)$ can be determined for any point in figure 3. The distributions of κ and $\tan\theta_0$ in these experiments provide a maximum $\delta_1 \Delta C_D$, at maximum κ, of 3.6×10^{-2}, with typical errors an order of magnitude smaller. Although all positive and non-cancelling, these $\delta_1 \Delta C_D$ would be barely perceptible in figure 4, and corrections have not been applied.

4.2. *Longitudinal oscillations of the sphere*

Longitudinal oscillations of the sphere are a source of error in reading $\tan\theta_0$ and of the scatter in figure 4. As noted earlier, these oscillations were not troublesome over most of the range of R and κ, although more severe with $\kappa = 0$ and becoming a limiting factor at lowest R for all κ. Acceleration and deceleration of the sphere were essentially completed within the first and last (the tenth) sections of the tank. The standard deviation of the eight readings of $\tan\theta_0$, $\sigma(\tan\theta_0)$, was computed for each pass in a sample of 64 passes well distributed over the range of R and κR shown in figure 2. These are the first passes of those experiments, at each value of $\Delta\rho/\rho_0$, with values of $10^{-2}R$ nearest 2, 4, 6, 10, 20, 40 and with smallest and largest R. In the unstratified case of $\Delta\rho/\rho_0 = 0$ the sample was doubled by including the second passes. In the 50 passes with stratification, $\sigma(\tan\theta_0)$ varied between 0.5 % and 4.4 % of the mean values of $\tan\theta_0$, with an average $\overline{\sigma(\tan\theta_0)}$ of 1.8 %. In the 14 passes without stratification, $\sigma(\tan\theta_0)$ varied between 2.1 % and 15.6 % of mean values, with a $\overline{\sigma(\tan\theta_0)}$ of 6.0 %. Further to confirm completion of acceleration within the first frame, the first values of $\tan\theta_0$ (taken during the second frame) from all these 64 passes were separated to obtain, for each pass, the ratio of the second-frame value to the eight-frame average, here denoted $\Delta_2 + 1$. In the 50 passes with stratification, the average of Δ_2, $\overline{\Delta_2}$, was +0.6 %, and its standard deviation $\sigma(\Delta_2)$ was 1.9 %. In the 14 passes without stratification, $\overline{\Delta_2}$ was −2.6 % and $\sigma(\Delta_2)$ was 7.1 %. The near equality of $\overline{\sigma(\tan\theta_0)}$ and $\sigma(\Delta_2)$ shows that by the start of the second frame $\tan\theta_0$ had effectively and consistently attained its constant value. When examined by separate values of $\Delta\rho/\rho_0$, it was found that $\overline{\sigma(\tan\theta_0)}$, although expectedly much reduced by the presence of stratification, was surprisingly little affected by its intensity. There is no indication that the longitudinal oscillations bias mean values of $\tan\theta_0$.

The severity of the longitudinal oscillations and the related scatter in the readings of $\tan\theta_0$ are plausibly linked (inversely) to the number of vortices shed per observation, that is, per frame of the tank. For the unstratified case, Achenbach (1974) gives the Strouhal number S over a range of R that includes these experiments (and reports multiple values beyond $R \sim 10^3$). Taking, roughly, the corresponding ranges $0.1 < S < 1.0$ for $1.5 \times 10^2 < R < 5 \times 10^3$, it is found that the number n of vortices shed in the length of a single frame has the corresponding range $2 < n < 20$. A tendency in these experiments for $\sigma(\tan\theta_0)$ to increase as R decreases at low values of R is most pronounced in the unstratified case. The suppression of longitudinal oscillations by stratification is plausibly caused by a suppression of vortex formation and shedding.

		All experiments	Young profiles	Old profiles	First passes
$\kappa < 1$	Sample size	153	41	31	30
	$\bar{\delta}$	0.0019	0.0010	0.0097	−0.0034
	$\sigma(\delta)$	0.024	0.023	0.030	0.014
$\kappa \geqslant 1$	Sample size	104	17	15	25
	$\bar{\delta}$	0.0082	0.0025	0.031	−0.0001
	$\sigma(\delta)$	0.089	0.054	0.103	0.069

TABLE 1. Averages and standard deviation of δ, the difference between a measured value of ΔC_D and the curve drawn in figure 4, for samples of experiments and passes in various categories

4.3. *Effects of boundaries and deteriorations of the profile*

The pattern of lee waves which spreads out behind the sphere remains undisturbed by the boundaries of the liquid and of the stratified region for, at least, some distance behind the sphere. Since this distance depends upon speed and stratification, which varied widely, the observed universal lack of dependence of $\tan\theta_0$ upon distance travelled by the sphere, as described in §4.2, would seem to imply a general negligibility of boundary effects upon D/W. This, in turn, would imply either that lee-wave reflections and disturbances at the boundaries had negligible effect on the drag, or that viscous dissipation effectively destroyed the lee waves before they could reach the boundaries.

Deterioration of the density profile is another possible source of error in determining ΔC_D and can be described as of two types. The first is the diffusion-related day-to-day shrinking of the region of nearly constant density gradient, described in §2.2. To explore its effects upon ΔC_D, for each filling of the tank, all experiments in the first 1, 2 or 3 days after filling, and the last 1, 2 or 3 days before emptying, were categorized as 'young profile' and 'old profile'. For each filling, the numbers of 'young' and 'old' days were equal and selected to keep the combined sample of experiments about 40 % of the total (within a range from 20 to 50 %). These categories, with their $\bar{\delta}$ and $\sigma(\delta)$, as defined in the first paragraph of §4, comprise the two middle columns in table 1. In the sequence 'young profile', 'all experiments', 'old profile', for both ranges of κ, both $\bar{\delta}$ and $\sigma(\delta)$ consistently increase. Here an effect of the deterioration becomes noticeable, but, comparing magnitudes of $\bar{\delta}$ and $\sigma(\delta)$ with ranges of ΔC_D in figure 4, it remains negligible. The second type of deterioration arises from mixing in the wake behind the sphere. This leaves a core of partially mixed liquid which then spreads laterally and thins vertically as molecular diffusion acts to heal the 'scar' in the profile. If the mixing is too severe, or the time between passes is too short, a distortion in the profile might build enough to affect the drag significantly. To verify that this was not the case, ΔC_D and δ were calculated separately for the first pass of each day, when the density profile was long undisturbed. This category, containing 55 passes, with its $\bar{\delta}$ and $\sigma(\delta)$, comprises the last column in table 1. An observed increase in $\bar{\delta}$ from 'first passes' to 'all experiments' is most likely a result of opposing residual currents left by previous passes in the latter category. In any case, again referring to figure 4, the differences in $\bar{\delta}$ and $\sigma(\delta)$ between the two categories are not significant.

4.4. *Errors in observing flow separation*

Overall errors in obtaining the angle of flow separation may be judged by the scatter in figure 6. Occasional lack of clarity in the polaroid photographs and frequent need for judgement made visual detection of separation the primary source of error, the subsequent calculation of ϕ being relatively accurate. This was based upon distances measured on a given photograph as it was mounted on a platform movable, by micrometer, normal to a fixed hairline. Orientation of the photograph provided displacements either along or normal to the path of the sphere. With the sideview shadowgraphs, avoiding large distortions along the path, and finding normal distortions to be kept negligible by the small angles of the light rays with the horizontal, ϕ was calculated from normal distances between separation points and the top and bottom of the sphere. In cases where the sphere was well past the station of the arclight, one of its rays, at a substantial angle with the perpendicular to the tank wall, would be tangent to the envelope of the wake and the surface of the sphere at two separate points. The resulting possible error in ϕ appears not to have been significant, since in figure 6 these data plot indiscriminately with those for the close-ups (marked by flags) in which the sphere was nearly on the perpendicular and this error was negligible. Also, the average difference in ϕ between upper and lower surfaces was essentially the same for the two sets of data. In the top-view dye-streak photographs and shadowgraphs, the images of the sphere and its shadow appeared round enough to neglect distortions. As ϕ remained fairly close to 90°, it was calculated from displacements measured along the path of the sphere between points of flow separation and points most forward and rearward on the sphere.

5. Interpretation of results

5.1. *Lee-wave drag, resonance and flow separation*

Even were the fluid inviscid, stratification would produce a drag on the sphere supplying a power input VD equal to the rate of increase of total energy contained in the lee waves behind it. The coefficient of this lee-wave drag, independent of R, is a function of κ. Presumably, in a real fluid, over some range of κ and R the drag coefficient is dominated by a positive lee-wave drag component dependent primarily upon κ, obviously the positive region of the curve in figure 4. The apparent mechanism of inviscid lee-wave drag is a deficit of pressure on the rear surface of the sphere as a downwash of fluid previously elevated by the passage of the sphere turns potential energy into an excess of kinetic energy.

This mechanism serves, roughly, to identify a maximum of $\Delta C_D/\kappa^2$ (rather than of ΔC_D) with a lee-wave resonance. In Brunt–Väisälä oscillations with vertical amplitude δ_m, the alternating maximum potential and kinetic energy, per unit volume, is $\frac{1}{2}\rho_0 N^2 \delta_m^2$. Assuming the average of this quantity to be the pressure deficit on the sphere, front-to-rear, provides the estimate

$$D \sim \tfrac{1}{2}\pi a^2 \rho_0 N^2 \overline{\delta_m^2}, \tag{11}$$

or, in dimensionless form,

$$\frac{\Delta C_D}{\kappa^2} \sim \frac{\overline{\delta_m^2}}{a^2}. \tag{12}$$

A maximum in $\Delta C_D/\kappa^2$, or $\overline{\delta_m^2/a^2}$, presumably occurs when δ_m/a for the largest

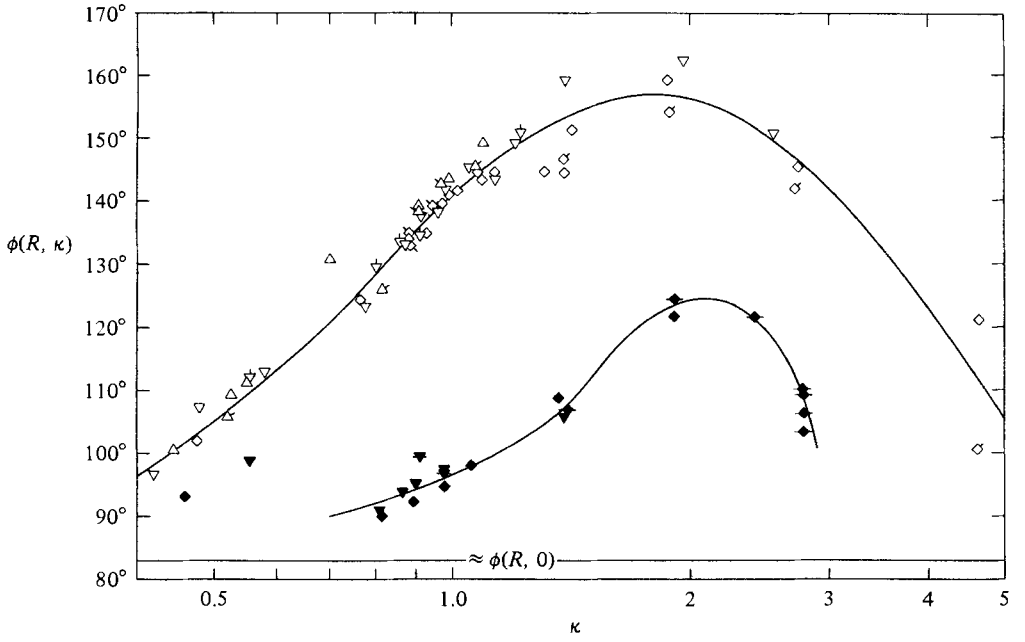

FIGURE 6. Delay in flow separation by stratification, in the vertical (open symbols) and horizontal (solid symbols) planes. Symbols are as in figures 3 and 4, with added flags and bars denoting close-up shadowgraphs and dye-streak photographs.

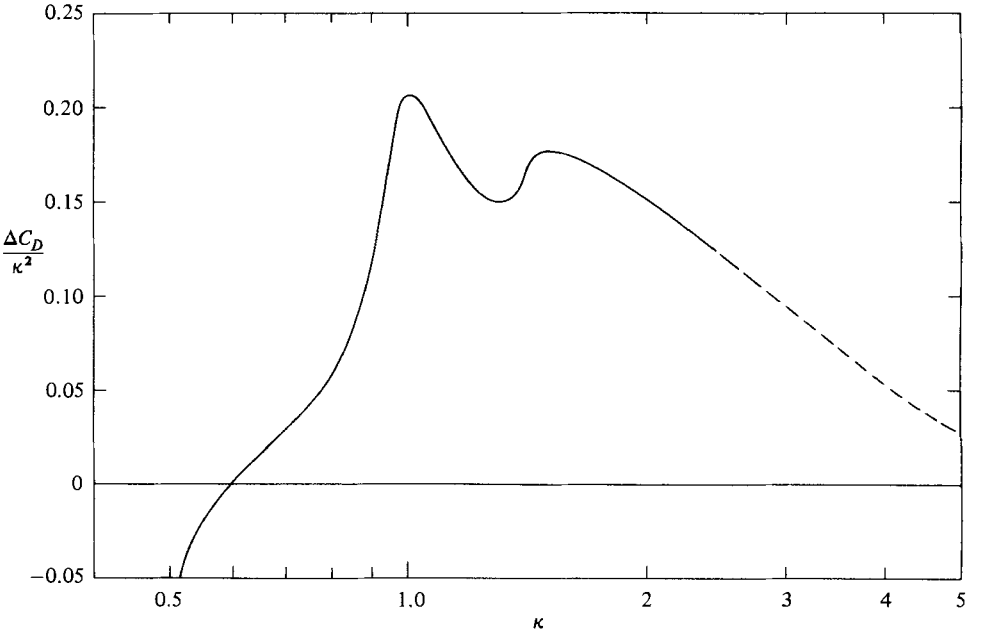

FIGURE 7. Observed $\Delta C_D/\kappa^2$, showing a general resonance maximum in the vicinity of $\kappa = \sqrt{2}$.

oscillation is a maximum. For the maximum oscillation, roughly between the crest of the sphere and the downstream track of its centre, $\delta_m \sim \frac{1}{2}a$, so that

$$\left(\frac{\Delta C_D}{\kappa^2}\right)_{\max} \lesssim \frac{1}{4}, \tag{13}$$

the inequality needed because δ_m^2 for the single maximum oscillation exceeds the maximum average of δ_m^2 over the area. The value of κ at which this maximum, or resonance, occurs can be estimated by requiring the unstratified downward acceleration of a particle a small distance above the sphere, $\sim V^2/a$, and starting the maximum oscillation, to equal the acceleration due to stratification at a crest, $\sim N^2\delta_m \sim \frac{1}{2}N^2a$. Thus

$$\kappa_{\text{resonance}} \sim \sqrt{2}. \tag{14}$$

The experiments support these rough arguments and their results reasonably well. In the second shadowgraph of figure 5, where $\kappa = 1.42$ is near the resonance value, $\sim \sqrt{2}$, the envelope of the wake approximates the maximum oscillation with wavelength $\lambda \approx V(2\pi/N)$, or with $\lambda/a \approx 2\pi/\kappa$, as in Brunt–Väisälä oscillations. In figure 7 the observed $\Delta C_D/\kappa^2$ is plotted against κ. (Division by κ^2 has amplified the undulations in ΔC_D to form the steep maximum near $\kappa = 1$.) It appears that (13) and (14) are in sufficient agreement with the observed height and position of the general maximum to permit its identification as a resonance in the lee-wave drag.

Compared with an unstratified separation angle $\phi(R,0)$ of around 83°, extrapolated from the subcritical range of R to the range of these experiments (Achenbach 1972, 1974), figure 6 shows that stratification delays separation, especially in the vertical plane. Depending upon κ, this delay can be large. It is an apparent consequence of the lee-wave drag, the point of separation tending to follow that of minimum pressure near that of maximum velocity outside the boundary layer. The smaller, but parallel, delay in separation in the horizontal plane is then a smaller response to the same cause. Both curves of $\phi(R,\kappa)-\phi(R,0)$ show some similarity to $\Delta C_D/\kappa^2$ in figure 7. No effect of R upon $\phi(R,\kappa)$ can be detected within the scatter of figure 6. It may be noted that the relationship between the lee-wave drag coefficient and ϕ contrasts with the combined steep drop in drag coefficient and increase in ϕ in the critical range of unstratified flow as the boundary layer becomes turbulent and thins and the flow outside becomes more like the potential flow around a sphere, without the rotational enhancement of downwash due to stratification.

5.2. *Turbulent suppression and drag reduction*

The descent of ΔC_D to negative values for small values of κ was unexpected, but can be interpreted as the result of a plausible mechanism. In a real fluid, part of the drag on the sphere is needed to pull along fluid within the separation surface behind it against the rearward pull of tangential stresses on this surface. Reduction of these stresses, or of the area on which they act, then plausibly reduces the drag. At the values of R accompanying the low values of κ where drag reduction was observed in these experiments, an unstratified wake and its stresses are largely turbulent. Suppression of vertical turbulent motions by stable stratification is to be expected because of the added potential energy which turbulent mixing must provide, and has been described by Lin & Pao (1979) in a review of past observations. The shadowgraphs in figure 5 further confirm this suppression in the relatively reduced vertical spreading of the wake. A reduced intensity of vertical turbulent motions implies reduced Reynolds stresses unless offset by more intense horizontal motions or by a higher

correlation between vertical and horizontal motions, a compensation made conceivable by enhanced local shear in the mean velocity. The observation of drag reduction then means that such compensations were not complete. A net drag reduction by suppression of turbulence emerges only as, far from resonance, the positive lee-wave drag subsides.

5.3. *Insensitivity of* ΔC_D to R

Insensitivity of ΔC_D to R, apparent in figure 4, is to be expected near the positive lee-wave resonance maximum, since lee-wave drag persists as the viscosity approaches zero, but continued insensitivity in the region of negative ΔC_D, where wake drag and viscous effects dominate, is surprising. Figure 3 shows that, in the region of R where negative values of ΔC_D were observed in these experiments, $C_D(R,0)$ is itself insensitive to R. Thus the present insensitivity suggests that $C_D(R,\kappa)$ might be expressed as a product of $C_D(R,0)$ and a function of κ. However, it is not known to what range of R such a relationship might be extended.

This work was partially supported by the Fluid Dynamics Program of the U.S. Office of Naval Research.

REFERENCES

ACHENBACH, E. 1972 Experiments on the flow past spheres at very high Reynolds numbers. *J. Fluid Mech.* **54**, 565–575.

ACHENBACH, E. 1974 Vortex shedding from spheres. *J. Fluid Mech.* **62**, 209–221.

DEBLER, W. & FITZGERALD, P. 1971 Shadowgraph observations of the flow past a sphere and a vertical cylinder in a density stratified liquid. *Tech. Rep.* EM-71-3, *Dept Engng Mech., Fluid Mech. Sect., Univ. Mich.*

LIN, J. T. & PAO, Y. H. 1979 Wakes in stratified fluids. *Ann. Rev. Fluid Mech.* **11**, 317–338.

PAO, H. P. & KAO, T. W. 1977 Vortex structure in the wake of a sphere. *Phys. Fluids* **20**, 187–191.

SCHLICHTING, H. 1968 *Boundary-Layer Theory*, 6th edn. McGraw-Hill.